Revealing the two distinctive roles of HY zeolite in enhancing the activity and durability of manganese oxide-zeolite hybrid catalysts for low-temperature NH$_3$-SCR

Hyun Sub Kim [a], Hwangho Lee [a], Hongbeom Park [a], Inhak Song [b,c,*], Do Heui Kim [a,**]

[a] School of Chemical and Biological Engineering, Institute of Chemical Processes, Seoul National University, Seoul 08826, Republic of Korea
[b] Department of Energy Environment Policy and Technology, Graduate School of Energy and Environment (KU-KIST Green School), Korea University, Seoul 02841, Republic of Korea
[c] Department of Integrative Energy Engineering, College of Engineering, Korea University, Seoul 02841, Republic of Korea

ARTICLE INFO

ABSTRACT

Recently, metal oxide-zeolite hybrid systems have shown promise in enhancing catalytic performance in low-temperature selective catalytic reduction (SCR), but not much is known as to mechanistic details. The purpose of this study is to examine fluctuations in low-temperature activity contingent upon the presence or absence of zeolite and to elucidate a dual functional mechanism of mixed zeolite in improving the catalytic performance of MnO$_x$, which is closely related to inter-particle diffusion of nitrite and nitrate species from MnO$_x$ to zeolite. Firstly, strong Brønsted acid sites on zeolite demonstrate a significantly faster reduction of diffused nitrite species compared to Brønsted/Lewis acid sites on MnO$_x$. More importantly, we discovered that zeolite prevents ammonium nitrate deposition by absorbing and decomposing diffused nitrate species from MnO$_x$. Such distinct interaction between zeolite and both nitrite and nitrate species clarified here will be of great promise in designing future hybrid catalytic materials for low-temperature NH$_3$-SCR reactions.

1. Introduction

Transition metal-based oxides have attracted great attention as effective catalysts for selective catalytic reduction with NH$_3$ (NH$_3$-SCR) at low temperatures, and many research has reported that, among those, MnO$_x$-based catalysts can operate effectively at low temperatures, approximately below 250 °C [1–3]. Despite the high catalytic performance of MnO$_x$-based catalysts compared to other oxide catalysts, the activity at low temperatures was insufficient to meet the rigorous regulations for NO$_x$ emissions. Therefore, catalyst modifications by introducing other metals as promoters have been adopted to improve the NH$_3$-SCR catalytic performance [4–6]. In 2003, Yang et al. reported that the cerium-modified MnO$_x$ catalyst synthesized via the citric acid method could significantly enhance catalytic activity compared to as-prepared MnO$_x$ and CeO$_x$ catalysts [7]. They also found that the MnCeO$_x$ catalyst has high resistance to H$_2$O and SO$_2$, exhibiting higher than 95 % NO$_x$ conversion in the presence of both H$_2$O and SO$_2$.

Notwithstanding such efforts to improve the catalytic performance, many MnO$_x$-based catalysts still suffer from inherent problems, such as (1) the deposition of ammonium nitrate (; AN, NH$_4$NO$_3$) that disrupts the long-term activity, (2) N$_2$O emission by decomposition of NH$_4$NO$_3$ that leads to low N$_2$ selectivity, and (3) resistance to H$_2$O and SO$_2$.

Apart from introducing promoters, many researchers have suggested hybrid catalytic systems consisting of a physical mixture of metal oxides and zeolites to solve the intrinsic problems of oxide catalysts [8–10]. The physical mixing method showed increased catalytic activity at low temperatures and enhanced durability compared to the case of using metal oxides or zeolite-based catalysts alone. The effect of the physical mixing was first reported by Misono et al., demonstrating the enhanced reduction rate of NO by C$_3$H$_6$ owing to the bifunctional mechanism via physically mixed Mn$_2$O$_3$ or CeO$_2$ with Ce-ZSM-5 samples [11]. Afterward, Sachtler et al. demonstrated that physically mixed H-form zeolite Y could decompose the impregnated ammonium nitrite (NH$_4$NO$_2$) on quartz [12]. This experiment suggested two mechanistic features of the

---

SCR reaction: First, nitrite species can undergo inter-particle diffusion with increasing temperatures. Second, the reduction of ammonium nitrite rapidly proceeds on the Brønsted acid sites, which is an important reaction step at the low-temperature range. Subsequently, Stakheeve et al. utilized the hybrid metal oxide-zeolite catalysts for the NH$_3$-SCR reaction and showed a significantly enhanced catalytic performance [13,14]. It was contended that the synergistic effect is ascribed to the NO oxidation over the metal oxide domain followed by fast-SCR reaction over zeolite-based catalysts. Grünert et al. also showed that the hybrid system could be an innovative way to enhance the catalytic performance in the NH$_3$-SCR reaction [15,16]. Contrary to the Stakheeve group, they asserted that the synergistic effect is not mediated by NO$_2$, which suggests that fast-SCR would not be the major contributor to the drastic synergistic effect of mixed zeolites. They speculated that the labile intermediate HNO$_2$ might be created over the oxidation component and would proceed with the additional reaction over the NH$_3$-SCR catalyst. Recently, Rappe et al. reported that enhanced low-temperature activity is attributable to the reaction between the nitrites/nitrate-precursors (e. g., HONO, N$_2$O$_3$) produced over metal oxides and NH$_4^+$ bound for Brønsted acid sites in the zeolite domain [17,18]. Although Cu ion-exchanged SSZ-13 zeolite was used in their study, a synergistic effect was observed as the zeolite with high Al content provides extra Brønsted acid sites. Obviously, the synergistic effect is consistently observed when metal oxides (or oxidation catalysts) and zeolite-based catalysts (or NH$_3$-SCR catalysts) have intimate contact by facile physical mixing. However, the mechanistic details of such synergistic effects are not completely understood and still debatable.

The good catalytic activity of MnO$_x$ at low temperatures is closely associated with the so-called fast-SCR reaction (NO+NO$_2$+2NH$_3$ → 2N$_2$+3H$_2$O) via NO activation since MnO$_x$ has excellent oxidation ability that facilitates NO oxidation at low temperatures compared to other metal oxides. It is widely accepted that, in a fast-SCR reaction, NO$_2$ undergoes dimerization (reaction (1)) and disproportionation (reaction (2)) at an early stage, and consecutive reaction (3) and reaction (4) proceed as such [19,20]:

$$2NO_2 \leftrightarrow N_2O_4 \tag{1}$$

$$N_2O_4 + H_2O \leftrightarrow HNO_2 + HNO_3 \tag{2}$$

$$NH_3 + HNO_2 \leftrightarrow NH_4NO_2 \rightarrow N_2 + 2H_2O \tag{3}$$

$$NH_3 + HNO_3 \leftrightarrow NH_4NO_3 \tag{4}$$
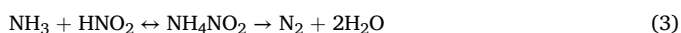
Considering the two different routes forming nitrite (or HNO$_2$) and nitrate (or HNO$_3$) species on catalysts, it is reasonable to investigate the reaction mechanism by focusing on the behavior of nitrite and nitrate species generated by reaction (2). However, many researchers have just reported that the excellent catalytic performance of MnO$_x$-based catalysts is simply related to the superior NO oxidation ability and other physicochemical properties [5,21]. At temperatures below 200 °C where the NH$_3$-SCR is investigated, adsorbed NO is activated into nitrite (NO$_2^-$) or nitrate (NO$_3^-$) on the surface and is not desorbed into gaseous NO$_2$. Therefore, in order to understand the mechanism of low-temperature SCR, it is necessary to deeply investigate how the oxidized forms of NO adsorbed on the surface (nitrite and nitrate species) participate in the reaction before desorbing as NO$_2$ at much higher temperatures. In this study, the time-resolved NH$_3$-SCR activity over MnO$_x$ at low temperatures was investigated in detail in the presence or absence of physically mixed HY zeolite. Based on NH$_3$-SCR reaction data and systematical temperature-programmed decomposition (TPD), we demonstrate that the physically mixed HY zeolites play two distinct roles: (1) the enhancement in low-temperature NH$_3$-SCR activity via diffusion of nitrite species and rapid decomposition of those intermediate species and (2) the inhibition of NH$_4$NO$_3$ deactivation via diffusion of nitrate species from MnO$_x$ to zeolite region, and subsequent reduction of those species by reaction with gaseous NO. The observed impacts of

co-locating zeolite in physical proximity to MnO$_x$ on the NH$_3$-SCR are complicated phenomena notably related to the diffusion of intermediate species. Our work will establish a foundational step in formulating high-performance hybrid metal oxide-zeolite catalysts, specifically designed for optimizing the NH$_3$-SCR reaction at low temperatures.

2. Experimental

2.1. Chemicals and reagents

Polyethylene glycol (PEG 3000), potassium permanganate (KMnO$_4$, ≥99.0 %), potassium chloride (KCl, 99.0–100.5 %), and NH$_4$NO$_3$ (≥99.0 %) were purchased from Sigma-Aldrich (USA). NH$_4^+$-form Y zeolite samples with varied Si/Al$_2$ ratios were acquired from Alfa Aesar (USA).

2.2. Catalyst preparation

MnO$_x$ was synthesized according to the previously reported method with some modifications [22]. In a typical synthesis, PEG 3000 (0.05 g) was dissolved in 100 mL of deionized water, and the solution was vigorously stirred for 10 min. Then, KMnO$_4$ (0.6 g) and KCl (0.1 g) were added to the PEG-containing solution. Subsequently, the mixture was heated in a Teflon-lined stainless steel autoclave at 170 °C for 4 h. The resulting brown powder was washed with 4 L of deionized water and dried at 105 °C overnight. The as-synthesized MnO$_x$ was calcined at 300 °C for 4 h with a ramping rate of 2 °C min^{-1}.

Before physical mixing, NH$_4^+$-form Y zeolite was calcined at 550 °C for 3 h. Then, the MnO$_x$ catalyst was physically mixed with HY zeolite by grinding in a mortar for 20 min, in which a mass ratio of MnO$_x$ and zeolite was 1:1 (denoted by MnO$_x$+Y(R), R = Si/Al$_2$ ratio).

2.3. Characterization

X-ray diffractometer (SmartLab, Rigaku, Japan), of which the X-ray wavelength is 1.54 Å with CuKα radiation, was utilized to collect X-ray diffraction (XRD) patterns of the samples. BELsorp (II)-mini (MicrotracBEL, Japan) was employed to obtain N$_2$ adsorption-desorption isotherms at 77 K using liquid N$_2$. The samples were pretreated under vacuum (< 10^{-2} kPa) at 120 °C for 12 h. The specific surface area was calculated using the Brunauer―Emmett―Teller (BET) equation. The morphological features of the samples were investigated with field emission scanning electron microscopy (FE-SEM; JSM-7800 F Prime, JEOL, Japan). Temperature-programmed reduction with H$_2$ (H$_2$-TPR) was conducted with a chemisorption analyzer (BELCAT II, MicrotracBEL, Japan). The sample was exposed to 5 % O$_2$ balanced with He at 200 °C for 1 h before implementing H$_2$-TPR analysis. Then, it was cooled down to 100 °C, and H$_2$ consumption was monitored with a thermal conductivity detector under 5 % H$_2$ balanced with He in the temperature range from 100 to 500 °C. Temperature-programmed desorption of NH$_3$ (NH$_3$-TPD) was performed with a chemisorption analyzer (BELCAT II, MicrotracBEL, Japan). Prior to NH$_3$-TPD, the sample was pretreated under He atmosphere at 200 °C for 1 h. Then, the sample was cooled down to 100 °C and saturated with NH$_3$. Subsequently, the sample was flushed with He for 1 h to eliminate the weakly adsorbed NH$_3$ species. Finally, the desorption process was conducted by increasing the temperature with a ramping rate of 10 °C min^{-1} in the temperature range from 100 °C to 750 °C. Fourier-transform infrared spectrometer (Nicolet 6700, Thermo Fisher Scientific, USA) was used to collect the *in situ* diffuse reflectance infrared Fourier transform spectroscopy (DRIFTS) spectra. The samples were pretreated with 5 % O$_2$ balanced with N$_2$ for 1 h at 300 °C and exposed to 500 ppm NO + 5 % O$_2$ for 1 h at 150 °C.

2.4. Measurement of catalytic activity

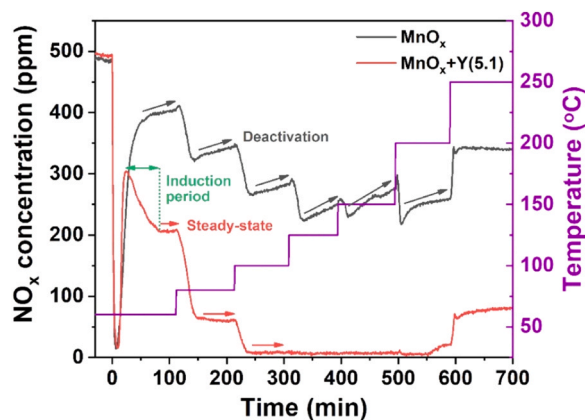After pelletizing and sieving the catalysts (180―250 μm), the NH$_3$-

Fig. 1. Time-resolved catalytic activity in NH$_3$-SCR reaction over MnO$_x$ and MnO$_x$+Y(5.1) samples. The reaction was performed with 500 ppm NO, 500 ppm NH$_3$, and 5 % O$_2$, balanced with N$_2$. The GHSV based on MnO$_x$ amount was 120,000 mL h^{-1} g^{-1}.

SCR reaction was conducted with 500 ppm NO, 500 ppm NH$_3$, and 5 % O$_2$, balanced with N$_2$. The total flow rate was 100 mL min^{-1} with 0.05 g of MnO$_x$ catalyst (gas hourly space velocity (GHSV) = 120,000 mL h^{-1} g^{-1}). When physically mixed samples were used, the NH$_3$-SCR reaction was performed with a 0.1 g catalyst (0.05 g MnO$_x$ + 0.05 g zeolite) to fix the amount of active material. All gas concentrations were determined by Fourier-transform infrared spectroscopy (FT-IR) spectrometer (Nicolet 6700, Thermo Fisher Scientific, USA) equipped with a 2 m gas cell. The conversion of NO$_x$ and selectivity to N$_2$ were calculated as follows:

$$NO_x conversion(\%) = \frac{[NO_x]_{in} - [NO_x]_{out}}{[NO_x]_{in}} \times 100$$

$$N_2 selectivity(\%) = \left[1 - \frac{2[N_2O]_{out}}{[NO_x]_{in} - [NO_x]_{out} + [NH_3]_{in} - [NH_3]_{out}}\right] \times 100$$

3. Results and discussion

3.1. Time-resolved NH$_3$-SCR activity of MnO$_x$ and MnO$_x$+Y(5.1) catalysts

Before investigating the NH$_3$-SCR activity, the as-synthesized MnO$_x$ catalyst was characterized by XRD, N$_2$ adsorption-desorption isotherm, and FE-SEM. The XRD peak positions of the as-prepared MnO$_x$ catalyst were consistent with the previously reported diffraction pattern [22], confirming that the δ-phase MnO$_2$ was well synthesized (Figure S1a). N$_2$ adsorption-desorption isotherm of the MnO$_x$ sample exhibited type-II isotherm (Figure S1b), of which the BET surface area and total pore volume were 77 m^2 g^{-1} and 0.23 cm^3 g^{-1}, respectively. The FE-SEM images of MnO$_x$ showed flower-like structures (Figure S1c,d), and the commercial Y zeolite exhibited faceted rectangular shapes (Figure S1e). After physical mixing, the two samples were uniformly mixed (Figure S1f), accompanying intimate contact between MnO$_x$ and zeolite Y. Subsequently, H$_2$-TPR experiments were conducted to investigate the reducibility of the catalysts (Figure S2). The MnO$_x$ sample exhibited one broad peak consisting of several MnO$_x$ reduction peaks, which are associated with the three-step reduction: MnO$_2$ to Mn$_2$O$_3$, Mn$_2$O$_3$ to Mn$_3$O$_4$, and Mn$_3$O$_4$ to MnO [23]. After grinding the MnO$_x$ sample in a mortar, the TPR profile of ground MnO$_x$ was almost unchanged compared to MnO$_x$, verifying that the grinding has no effect on the average oxidation state and reducibility of MnO$_x$ itself. However, the H$_2$-TPR profile of the MnO$_x$+Y(5.1) sample was separated into two broad peaks, suggesting that the strong interaction between MnO$_x$ and Y (5.1) was formed during the physical mixing procedure. The observed interaction could be due either to (1) the intimate contact of MnO$_x$ with the HY zeolite leading to ion exchange with the Brønsted acid sites of the HY zeolite under a reducing atmosphere and/or (2) the formation of Si (Al)−O−Mn bonds facilitating metal-support interactions. Considering that the H$_2$-TPR profile of MnO$_x$+Y(5.1) exhibited differences with that of MnO$_x$ above 320 °C, it can be inferred that the reduced Mn species could interact strongly with HY zeolite. Furthermore, the H$_2$-TPR profile of the simply shaken MnO$_x$+Y(5.1)_S sample, in which two powder samples were not ground in a mortar but just mixed in a reactor by hand, showed a profile similar to that of MnO$_x$, suggesting that the physical mixing process is essential for forming the interactions mentioned earlier.

The catalytic activity in NH$_3$-SCR reaction is generally reported based on steady-state NO$_x$ concentration. However, as reported by Dong et al., the catalytic activity of the MnO$_x$ sample deteriorated as the reaction time elapsed [24], resulting from the continuous deposition of intermediate NH$_4$NO$_3$ species that physically block the active sites of the catalysts. Therefore, we investigated the time-resolved NH$_3$-SCR activity of MnO$_x$ and physically mixed MnO$_x$+Y(5.1) samples, as shown in Fig. 1. The significant decrease in NO$_x$ concentration was monitored when the reactant gases began to flow from the bypass to the MnO$_x$ catalyst at 60 °C. Subsequently, it increased to approximately 380 ppm, and continuous deactivation was observed along the elapsed reaction time. Such gradual decline in activity, i.e., deactivation of the catalytic activity by deposition of NH$_4$NO$_3$, was observed not only at 60 °C but at increased temperatures (80—200 °C). The deterioration was not observed at 250 °C since NH$_4$NO$_3$ could easily decompose at 250 °C over MnO$_x$ (see Fig. 6). Similar to the MnO$_x$ sample, the initial NO$_x$ concentration was significantly decreased for the MnO$_x$+Y(5.1) sample and increased to approximately 300 ppm. Then, the NO$_x$ concentration further decreased to 200 ppm, showing a different trend from MnO$_x$, and it reached a steady-state in about 60 min without any deactivation as time elapsed. In other words, a distinctive phase, akin to an induction period, was exclusively discerned only for the MnO$_x$+Y(5.1) sample when reactants were introduced to the catalysts. Furthermore, the decrease in catalytic activity was not monitored at all as the reaction time increased for the case of the MnO$_x$+Y(5.1) sample when the reaction temperature increased to even higher temperatures. Hence, it is conceivable that the deactivation induced by NH$_4$NO$_3$ deposition was mitigated through the incorporation of HY zeolite. Moreover, it is worth noting that the catalytic performance was considerably improved upon introducing zeolite by the facile physical mixing method. In the ensuing results, we will explain (i) why gradual isothermal deactivation is not observed in hybrid catalysts and (ii) why an induction period is observed for enhanced SCR activity to occur and be stabilized.

3.2. Water in zeolite retards the participation of nitrite (NO$_2^-$) intermediates

3.2.1. Time-resolved activity of catalysts under different conditions

One of the major intermediate species in NH$_3$-SCR reaction over MnO$_x$ is reported as NH$_4$NO$_2$, which is produced via reaction (3), and it is well known that the NH$_4$NO$_2$ promptly decomposes to N$_2$ and H$_2$O [25]. Prompt decomposition pathway after N-N coupling is also similarly observed in the reaction between oxidized NO (NO$^+$) and NH$_3$ over H zeolites [26]. Even in the absence of a catalyst, NH$_4$NO$_2$ decomposition proceeds readily at approximately 100 °C. As reported by Sachtler et al., the NH$_4$NO$_2$ decomposition reaction could be accelerated by the solid acid catalyst with Brønsted acid sites, which can provide the protons [12]. They demonstrated via temperature-programmed decomposition of NH$_4$NO$_2$ experiments that the decomposition of NH$_4$NO$_2$ impregnated on quartz powder was promoted by HY zeolite close-contacted with NH$_4$NO$_2$/quartz via a physical mixing procedure. It indicates that even though the Brønsted acid sites are provided as a form
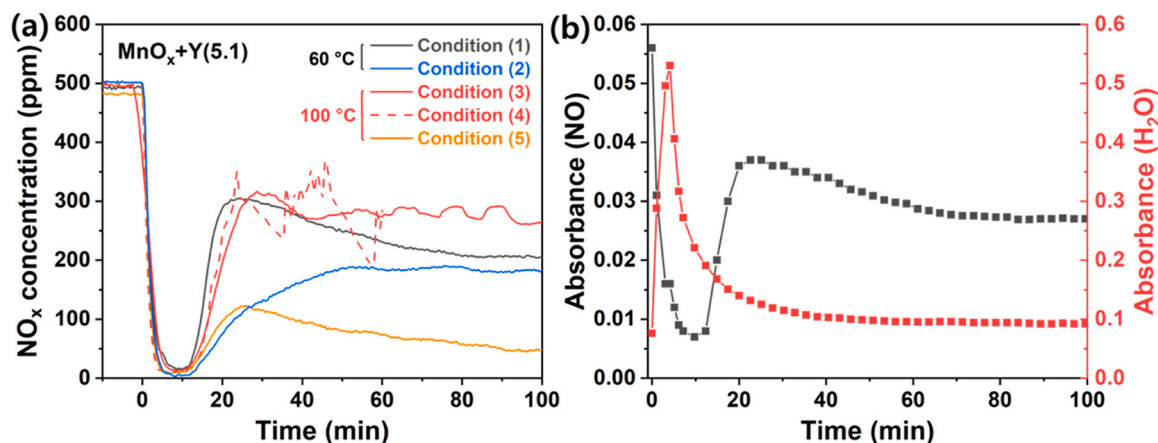
Fig. 2. (a) NH$_3$-SCR activity over MnO$_x$+Y(5.1) sample with various reaction conditions; (1) the reaction was conducted under dry conditions at 60 °C, (2) the catalyst was pretreated at 300 °C for 1 h and the reaction was conducted under dry conditions at 60 °C, (3) the reaction was conducted at 100 °C with 2 vol% H$_2$O, (4) the sample was saturated with 2 vol% H$_2$O and the reaction was conducted at 100 °C with 2 vol% H$_2$O, and (5) the sample was saturated with 2 vol% H$_2$O and the reaction was conducted at 100 °C in the absence of H$_2$O. (b) The absorbance profiles of NO and H$_2$O that correspond to condition (1).

of the physical mixture, it facilitates the rapid decomposition of NH$_4$NO$_2$ located in other domains. Therefore, the significantly enhanced catalytic activity of the MnO$_x$+Y(5.1) sample could be ascribed to the fast decomposition of the diffused nitrite species, exclusively produced over the MnO$_x$ active site, on the Brønsted acid sites of HY zeolite.

To elucidate the origin of the induction period over hybrid catalysts, we investigated the time-resolved catalytic performance of NH$_3$-SCR over the MnO$_x$+Y(5.1) sample under various reaction conditions (Fig. 2a). Without any pretreatment, the MnO$_x$+Y(5.1) sample exhibited the induction period at 60 °C, and it took approximately 80 min for the activity to be stabilized and approached to the steady-state (condition (1)). For comparison, H$_2$O was eliminated by pretreating the MnO$_x$+Y (5.1) sample with air at 300 °C for 1 h, and the NH$_3$-SCR was conducted at 60 °C in the absence of H$_2$O (condition (2)). After removing water from zeolite, the NO$_x$ concentration was sharply decreased and gradually increased to 200 ppm, reaching a steady-state only after 50 min. Moreover, no induction period was observed after pretreatment, indicating that the presence of water inside HY zeolite could reduce the enhancement in catalytic activity at the early stage of the NH$_3$-SCR reaction. The retarded reaction rate over MnO$_x$+Y(5.1) in the presence of H$_2$O could be potentially attributable to (1) a decreased diffusion rate of nitrite species toward the zeolite domain and/or (2) a delay of the reaction rate between nitrite species and ammonium ions adsorbed on

Brønsted acid sites. Therefore, the diffusion rate of nitrite species and/or their N-N coupling with ammonium ions seems to be crucial for metal oxide-zeolite hybrid catalysts, and the diffusion of nitrite species from the MnO$_x$ surface to the zeolite domain and/or N-N bond formation between nitrite and ammonium ions in zeolite seems to be hindered in the presence of H$_2$O. When the NH$_3$-SCR reaction was conducted in the presence of 2 vol% H$_2$O at 100 °C without pretreatment (condition (3)), no such induction period was observed because zeolite always remained as saturated with water. While the decreased catalytic activity under humid conditions could be generally ascribed to the competitive adsorption of reactants and H$_2$O [27], it can be deduced that these phenomena could also be attributable to the decreased diffusion rate of nitrite species and/or the retarded formation of NH$_4$NO$_2$ intermediate. In the case of the sample saturated with 2 vol% H$_2$O for 1 h before the NH$_3$-SCR reaction (condition (4)), the NH$_3$-SCR result with 2 vol% H$_2$O at 100 °C was too oscillated to check qualitatively the existence of the induction period and NO$_x$ conversion. Afterward, the sample was saturated with 2 vol% H$_2$O for 1 h at 100 °C, and the reaction was carried out under dry conditions (condition (5)). It exhibited the induction period for the initial stage of the NH$_3$-SCR reaction, also implying that the presence of H$_2$O in zeolite hindered the diffusion of nitrite and/or formation of NH$_4$NO$_2$, thereby resulting in the induction period until most of the water is desorbed by flowing dry feed. Moreover, we
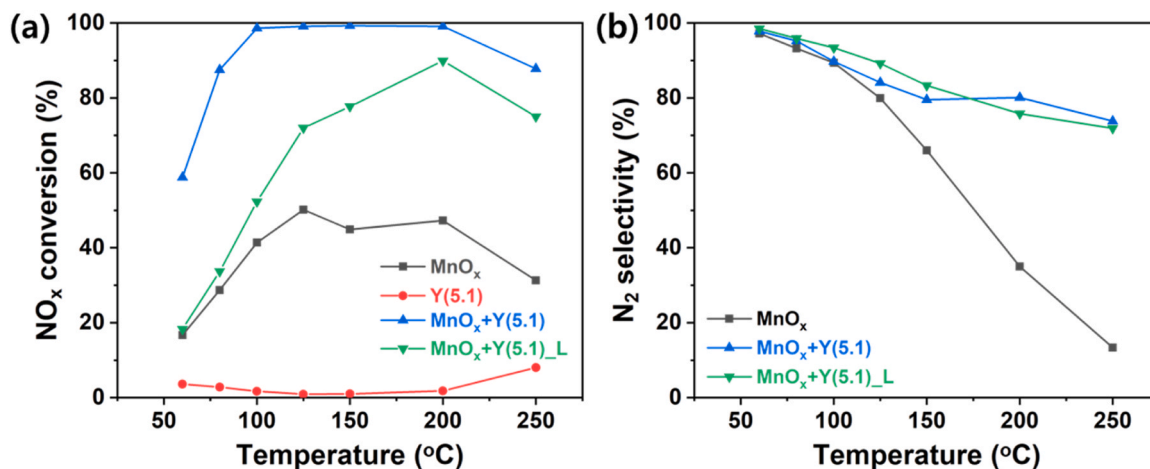

Fig. 3. (a) NO$_x$ conversion of MnO$_x$, Y(5.1), MnO$_x$+Y(5.1), and MnO$_x$+Y(5.1)_L and (b) N$_2$ selectivity of MnO$_x$, MnO$_x$+Y(5.1) and MnO$_x$+Y(5.1)_L samples in NH$_3$-SCR reaction. The reaction was performed with 500 ppm NO, 500 ppm NH$_3$, and 5 % O$_2$, balanced with N$_2$. The GHSV based on MnO$_x$ amount was 120,000 mL h^{-1} g^{-1}.

Fig. 4. (a) NO_x conversion and (b) N_2 selectivity of MnO_x+Y(5.1), MnO_x+Y(30), and MnO_x+Y(80) samples in NH_3-SCR reaction. The reaction was performed with 500 ppm NO, 500 ppm NH_3, and 5 % O_2, balanced with N_2. The GHSV based on MnO_x amount was 120,000 mL h^{-1} g^{-1}.
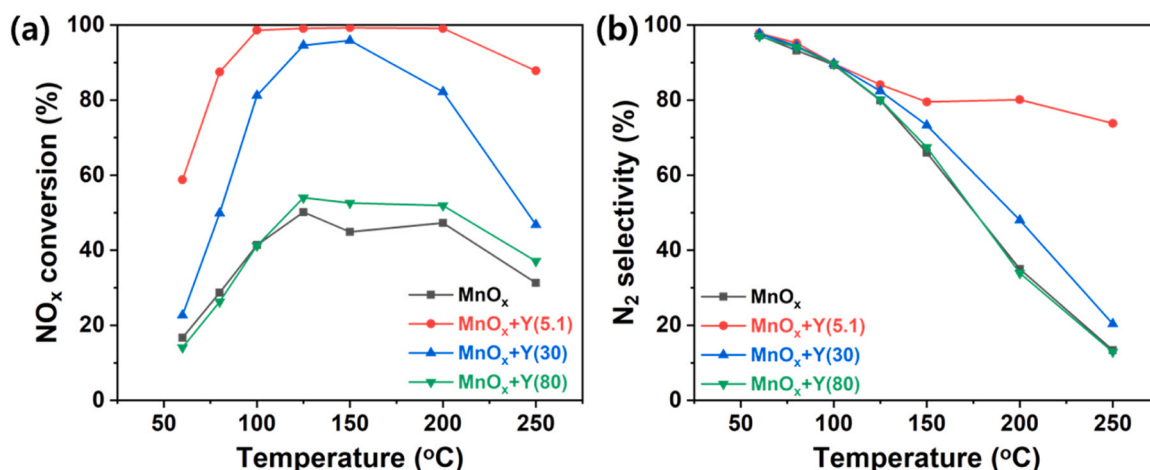
cross-checked the NO and H_2O bands in IR spectra, as shown in Fig. 2b. When reactants were fed to the sample, the absorbance signal of H_2O was drastically increased because of the simple desorption of H_2O in the zeolite structure. Then, as NO_x concentration approached a steady-state, the H_2O absorbance signal was also stabilized, demonstrating the clear correlation between the amount of desorbing water and NO removal rate.

3.2.2. Acid sites on zeolite adjacent to MnO_x are required for consuming diffused nitrite species

The steady-state reached activities of the prepared catalysts at temperatures from 60 to 250 °C are plotted in Fig. 3, in which the NO_x conversion of MnO_x was obtained from the last 5 min data before the temperature ramp. The NO_x conversion of MnO_x gradually increased and reached 50 % at 125 °C, and it showed seagull-like decreasing trends, exhibiting 31 % at 250 °C. The N_2 selectivity of MnO_x decreased progressively from 97 % to 13 % in the temperature range from 60 to 250 °C. HY zeolite without Mn components exhibited negligible catalytic performance, below 4 % NO_x conversion up to 200 °C and 8 % at 250 °C. When MnO_x was physically mixed with HY zeolite, the catalytic activity was drastically increased compared to individual components, MnO_x and HY zeolite, and it was far beyond the algebraic sum of those NO_x conversions. MnO_x+Y(5.1) catalyst exhibited 88 % conversion at 80 °C and approximately 100 % conversion from 100 to 200 °C. It is worth noting that the N_2 selectivity of the MnO_x+Y(5.1) sample was also significantly improved compared to the MnO_x catalyst at temperatures higher than 125 °C, and it increased from 13 % to 74 %, especially at 250 °C. Subsequently, the MnO_x and Y(5.1) were sieved separately and mixed by shaking them softly in the reactor, denoted by MnO_x+Y(5.1)_L; this sample also showed a synergistic effect to some extent but attenuated compared to that of the intimately contacted MnO_x+Y(5.1) sample. It indicates that the diffusion of nitrite species toward the zeolite domain via intimate contact of two samples is a crucial factor determining the catalytic activity. Although MnO_x can readily oxidize adsorbed NO to nitrite species on its surface, the absence of strong acid sites for ammonium nitrite reduction limits NO removal rate at low temperatures. The HY zeolite, adjacent to the MnO_x surface for facile nitrite diffusion, can boost the NO removal rate by providing abundant acid sites. Moreover, it is noticeable that the trend of the N_2 selectivity over MnO_x+Y(5.1)_L is similar to MnO_x+Y(5.1) sample rather than MnO_x. It suggests that the reaction intermediate species would likely decompose over the zeolite domain via Brønsted acid sites since N_2O formation that primarily contributes to N_2 selectivity was significantly decreased (*vide infra*).

Then, the NH_3-SCR reaction was conducted with the MnO_x+Y

samples having different Si/Al_2 ratios (Fig. 4). When the MnO_x was physically mixed with zeolite Y(30), the extent of improved catalytic activity and N_2 selectivity was inferior to that of MnO_x+Y(5.1). The MnO_x+Y(80) sample showed NO_x conversion and N_2 selectivity that were almost similar to MnO_x. In other words, the enhancement in catalytic performance was not observed, though there was intimate contact between MnO_x and Y(80). That is, the Si/Al_2 ratio of the zeolite is a critical factor that determines the enhancement of the catalytic performance of physically mixed catalysts. As the content of Al present in zeolite Y decreases, which means that the number of Brønsted acid sites decreases and becomes hydrophobic [28], the effect of synergistic enhancement weakens. As shown in Figure S3, the total amount of acid sites of zeolite Y(5.1) (3.677 mmol/g) significantly exceeded those of zeolite Y(30) (0.852 mmol/g) and Y(80) (0.499 mmol/g) samples. In addition, when the amount of HY zeolite was reduced while the Si/Al_2 ratio was fixed at 5.1, the NO_x conversion and N_2 selectivity were decreased at a temperature higher than 150 °C (Figure S4). Therefore, it can be inferred that a certain amount of acid sites are required to decompose NH_4NO_2 generated through the diffusion of nitrite species. The insufficient number of acid sites limits the NO removal rate, indicating that the diffusion of nitrite species or their decomposition on zeolite acid sites is much slower than the NO activation step occurring on the MnO_x surface. The N_2 selectivity was deeply influenced by the zeolite Si/Al_2 ratio, in which the zeolite Y(30) and Y(80) exhibited low N_2 selectivity compared to the Y(5.1) sample. It also corroborates that the NO activation over MnO_x is faster than the diffusion and decomposition of nitrite species over zeolite. If NO oxidation were a slower process, the degradation of NH_4NO_2 would have occurred immediately, enhancing N_2 selectivity. In previous data (Fig. 2), the presence of water in zeolite negatively affected the NO removal rate, where the rate-limiting step was the diffusion/decomposition of nitrite species on the acid sites in zeolite. However, zeolite with abundant Brønsted acid sites has a problem in that it readily exists in a hydrated state at low temperatures due to its good hydrophilicity. Thus, such a relationship between acidity and hydrophilicity of zeolite must be well controlled in order to optimize the low-temperature SCR reaction rate.

3.3. Adjacent zeolites alleviate ammonium nitrate (NO_3) deactivation of Mn oxides

3.3.1. Observation of ammonium nitrate deactivation

Along with the diffusion of nitrite species and accelerated decomposition of NH_4NO_2 by zeolite adjacent to MnO_x, it should be noted that the deterioration of NO_x conversion as reaction time elapsed was observed consistently over MnO_x. Contrary to the MnO_x sample, the
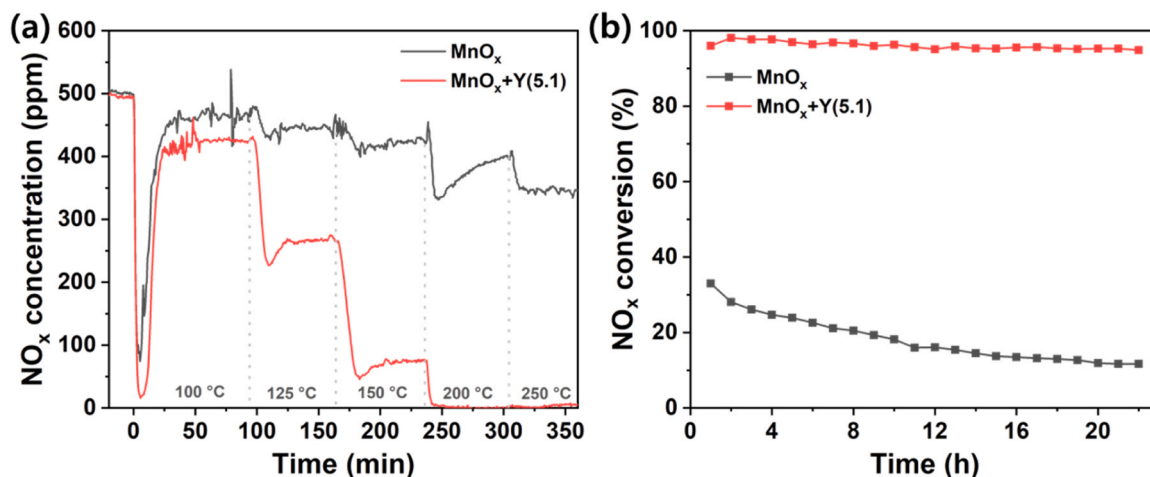
Fig. 5. (a) Time-resolved catalytic activity (b) long-term activity in NH$_3$-SCR reaction over MnO$_x$ and MnO$_x$+Y(5.1) samples. The reaction was performed with 500 ppm NO, 500 ppm NH$_3$, and 5 % O$_2$ in the presence of 5 % H$_2$O for time-resolved activity and in the absence of H$_2$O for long-term activity. The GHSV based on MnO$_x$ amount was 120,000 mL h^{-1} g^{-1} and 360,000 mL h^{-1} g^{-1} for time-resolved activity and long-term activity, respectively.
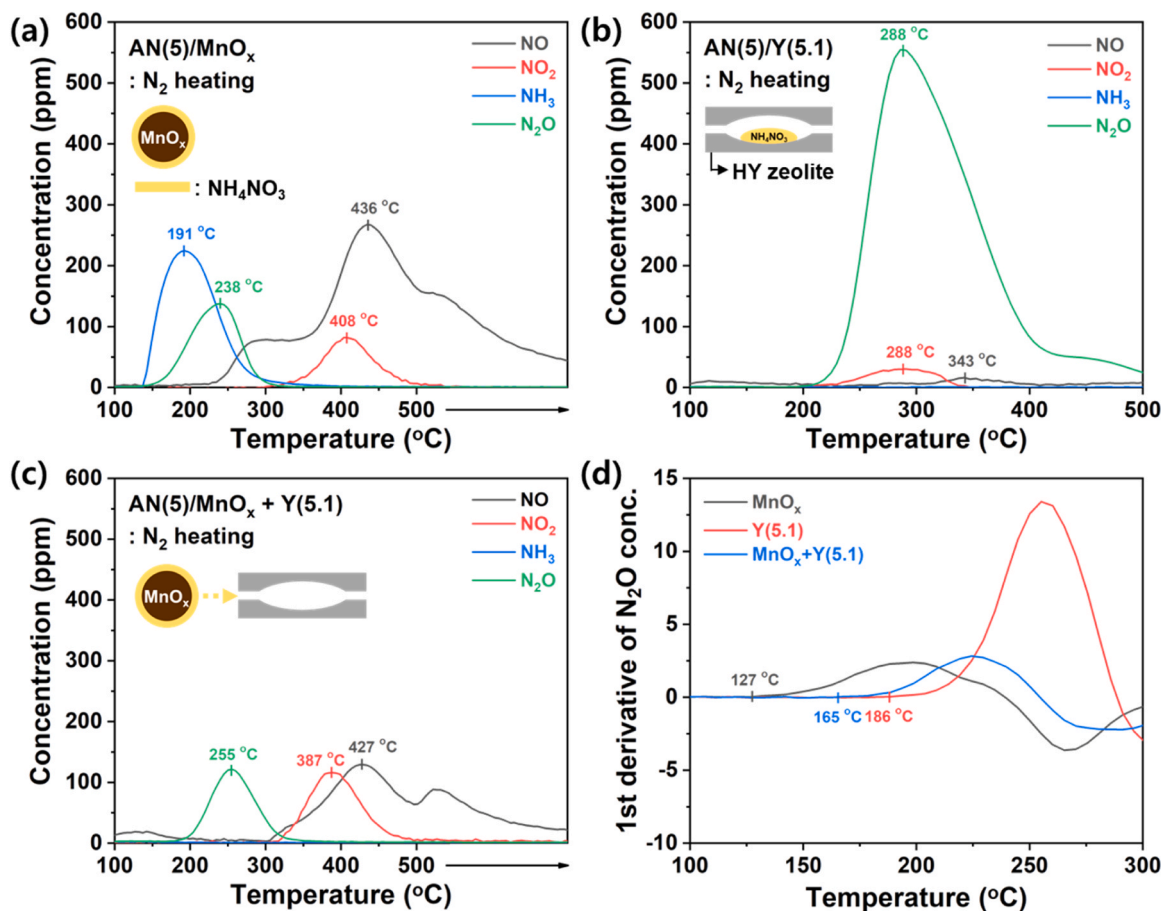

Fig. 6. The concentration profiles of temperature-programmed decomposition over (a) AN(5)/MnO$_x$, (b) AN(5)/Y(5.1), and (c) AN(5)/MnO$_x$+Y(5.1), which was conducted under N$_2$ atmosphere. The corresponding 1st derivative of N$_2$O concentration profiles is in (d).

exacerbation of NO$_x$ conversion was clearly not observed over MnO$_x$+Y (5.1) (Fig. 1). As shown in Fig. 5a, the NH$_3$-SCR reaction was also conducted in the presence of 5 vol% of H$_2$O over the MnO$_x$ and MnO$_x$+Y (5.1) samples to observe the ammonium nitrate deactivation in the presence of water. Although the extent of deactivation was not severe, catalytic activity slowly decreased over the elapsed time at 150 °C, demonstrating the deposition of NH$_4$NO$_3$ on active sites [24]. An

increase in temperature to 200 °C caused severe deactivation, in which NO oxidation and NH$_3$-SCR reaction proceed vigorously compared to at 150°C. However, the deterioration of catalytic activity was not monitored at 250 °C since NH$_4$NO$_3$ commences to decompose over MnO$_x$ at lower than 250 °C (see Fig. 6). Compared to the reaction conditions in the absence of H$_2$O (Fig. 1), severe deactivation was not observed over MnO$_x$ at 100 and 125 °C. This is because NO activation does not proceed
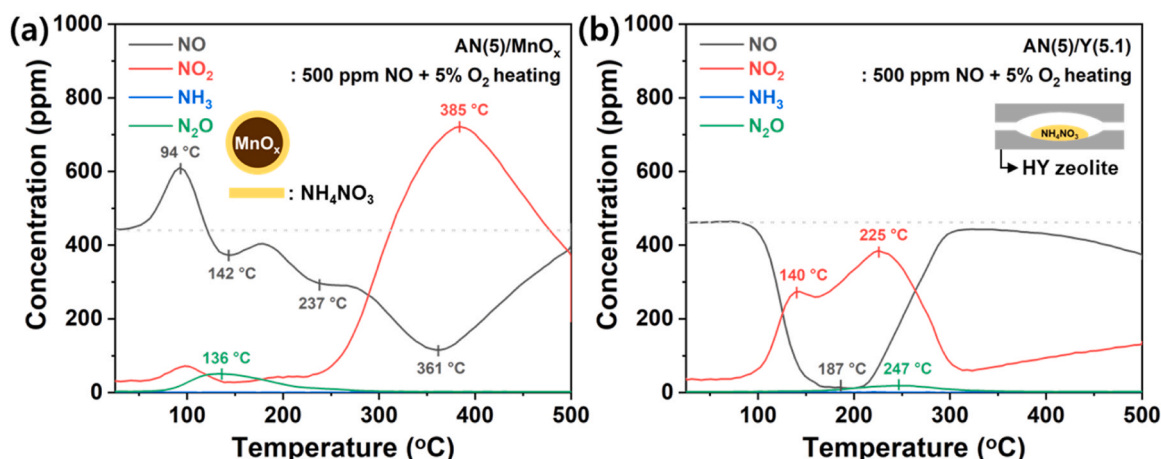
Fig. 7. The concentration profiles of temperature-programmed decomposition over (a) AN(5)/MnO$_x$ and (b) AN(5)/Y(5.1) under 500 ppm NO + 5 % O$_2$.

actively in the presence of H$_2$O, thereby suppressing the formation of NH$_4$NO$_3$. Indeed, the NO oxidation ability over MnO$_x$ was atrocious, exhibiting almost below 1 % NO to NO$_2$ conversion, even in the absence of H$_2$O (Figure S5). It is notable that when the NH$_3$-SCR reaction proceeds vigorously enough (especially at 200 and 250 °C), the N$_2$ selectivity of MnO$_x$ in the presence of H$_2$O was superior to that in the absence of H$_2$O (see Fig. 3 and S6). Since NH$_4$NO$_2$ produced over MnO$_x$ is decomposed into N$_2$ and H$_2$O even at low temperatures, the increased N$_2$ selectivity seems to be concerned with NH$_4$NO$_3$ that decomposed into N$_2$O and H$_2$O. The MnO$_x$+Y(5.1) sample exhibited enhanced NO$_x$ conversion and N$_2$ selectivity compared to the MnO$_x$ sample, even in the presence of 5% water, as shown in Figure S6. It is noticeable that the deterioration in catalytic activity as time elapsed was hardly observed for the MnO$_x$+Y(5.1) sample. Considering retardation in deactivation by NH$_4$NO$_3$ and the significant enhancements in N$_2$ selectivity, we strongly suppose that HY zeolite adjacent to MnO$_x$ affects the behavior of not only nitrite species but directly nitrate species. As nitrite species formed over MnO$_x$ could be diffused to the zeolite domain, nitrate species might also have migrated toward the zeolite domain, contributing to resulting catalytic performance.

3.3.2. Direct evidence of inter-particle migration of nitrates species

Our previous research found that the NH$_3$-NO$_3$ intermediate can be stabilized in small-pore structures [29], resulting in the suppressed decomposition of intermediate species. That is, the formation of N$_2$O by decomposition of NH$_4$NO$_3$ will be retarded, contributing to enhancement in N$_2$ selectivity. These NH$_4$NO$_3$, confined in a small-pore structure, could be reduced by NO to produce NH$_4$NO$_2$ and NO$_2$, followed by decomposition of NH$_4$NO$_2$ into N$_2$ and H$_2$O and, improving the NO$_x$ conversion and N$_2$ selectivity (reaction (5)).

$$NH_4NO_3 + NO \rightarrow NH_4NO_2 + NO_2 \rightarrow N_2 + NO_2 + 2H_2O \quad (5)$$
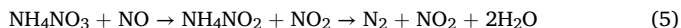
First, we conducted temperature-programmed decomposition (TPD) to investigate the decomposition behavior of NH$_4$NO$_3$ on MnO$_x$ and zeolite Y(5.1). The 5 wt% NH$_4$NO$_3$ was impregnated over MnO$_x$ (AN(5)/MnO$_x$) and zeolite Y(5.1) (AN(5)/Y(5.1)). Then, AN(5)/MnO$_x$ was physically mixed with zeolite Y(5.1) to observe the migration of nitrate species. The TPD experiments were carried out under an N$_2$ atmosphere, in which the following reactions can be entailed for the thermal decomposition of NH$_4$NO$_3$ [30]:

$$NH_4NO_3 \leftrightarrow NH_3 + HNO_3 \quad (6)$$

$$NH_4NO_3 \rightarrow 0.5N_2 + NO + 2H_2O \quad (7)$$

$$NH_4NO_3 \rightarrow N_2O + 2H_2O \quad (8)$$

It is well-known that the thermal decomposition of NH$_4$NO$_3$ commences with an endothermic proton transfer reaction, which results in the formation of NH$_3$ and HNO$_3$ (reaction (6); reverse reaction (4)). Then, the exothermic decomposition, which produces N$_2$, NO, and H$_2$O, arises approximately at 200 °C (reaction (7)). Above 230 °C, NH$_4$NO$_3$ can be decomposed irreversibly into N$_2$O and H$_2$O (reaction (8)), which is generally attributed to the low N$_2$ selectivity of Mn-based oxide catalysts.

When TPD was conducted with AN(5)/MnO$_x$ under an N$_2$ atmosphere (Fig. 6a), the NH$_3$ peak was observed at 191 °C, which is ascribed to the results of the reaction (6), and the N$_2$O peak was monitored at 238 °C as a result of the reaction (8). Then, the broad peaks for NO consisting of some shoulder peaks via reaction (7) and NO$_2$ peak were detected at 436 and 408 °C, respectively. The NO$_2$ peak arises from the NO oxidation over the MnO$_x$ catalyst. For the AN(5)/Y(5.1) sample (Fig. 6b), the NH$_3$ was not detected, and a small amount of NO was detected at 343 °C, implying that the reaction (6) and (7) were suppressed. A significant amount of N$_2$O was released because of the reaction (8), and the corresponding N$_2$O peak appeared at 288 °C. Note that the N$_2$O peak over AN(5)/Y(5.1) was shifted toward a higher temperature than that over the AN(5)/MnO$_x$ sample. It demonstrates that the NH$_4$NO$_3$ is more stable and exhibits totally different decomposition behavior when it is located in HY zeolite with a microporous structure than when it exists on the surface of the MnO$_x$. Furthermore, there was a clear difference in the temperature at which the degradation of NH$_4$NO$_3$ was initiated, as shown in Fig. 6d. From the first derivative curves of N$_2$O concentration profiles, the degradation of NH$_4$NO$_3$ via reaction (8) was started at 127 °C for the MnO$_x$ sample, whereas at 186 °C for the Y(5.1) sample, ensuring the stabilization of NH$_4$NO$_3$ by the micropore structures. Although the AN(5)/MnO$_x$+Y(5.1) sample exhibited similar concentration profiles to that of AN(5)/MnO$_x$ for N$_2$O and NO$_2$ (peaks at 255 and 387 °C, respectively) (Fig. 6c), the NH$_3$ was not detected, and the released NO amount was significantly decreased. It can be deduced that the NH$_3$-SCR reaction proceeded between NH$_3$ and NO formed by the decomposition of NH$_4$NO$_3$. Note that even though the NH$_4$NO$_3$ was impregnated on MnO$_x$, not on zeolite Y, the N$_2$O peak position was shifted toward a higher temperature (255 °C) compared to that of AN(5)/MnO$_x$ (238 °C). In addition, the starting point of NH$_4$NO$_3$ degradation was also shifted toward a higher temperature (165 °C), close to the decomposition temperature via zeolite Y (186 °C), compared to AN(5)/MnO$_x$ (127 °C). Therefore, it could be surmised that the nitrate species was partially diffused from MnO$_x$ to the adjacent HY zeolite domain during these simulated N$_2$-TPD experiments.

Then, the TPD was conducted in an atmosphere of 500 ppm NO + 5 % O$_2$ over AN(5)/MnO$_x$ and AN(5)/Y(5.1) samples, more analogous to the reaction atmosphere (Fig. 7). The NO and NO$_2$ peaks were observed at approximately 100 °C for AN(5)/MnO$_x$, denoting that the NO was
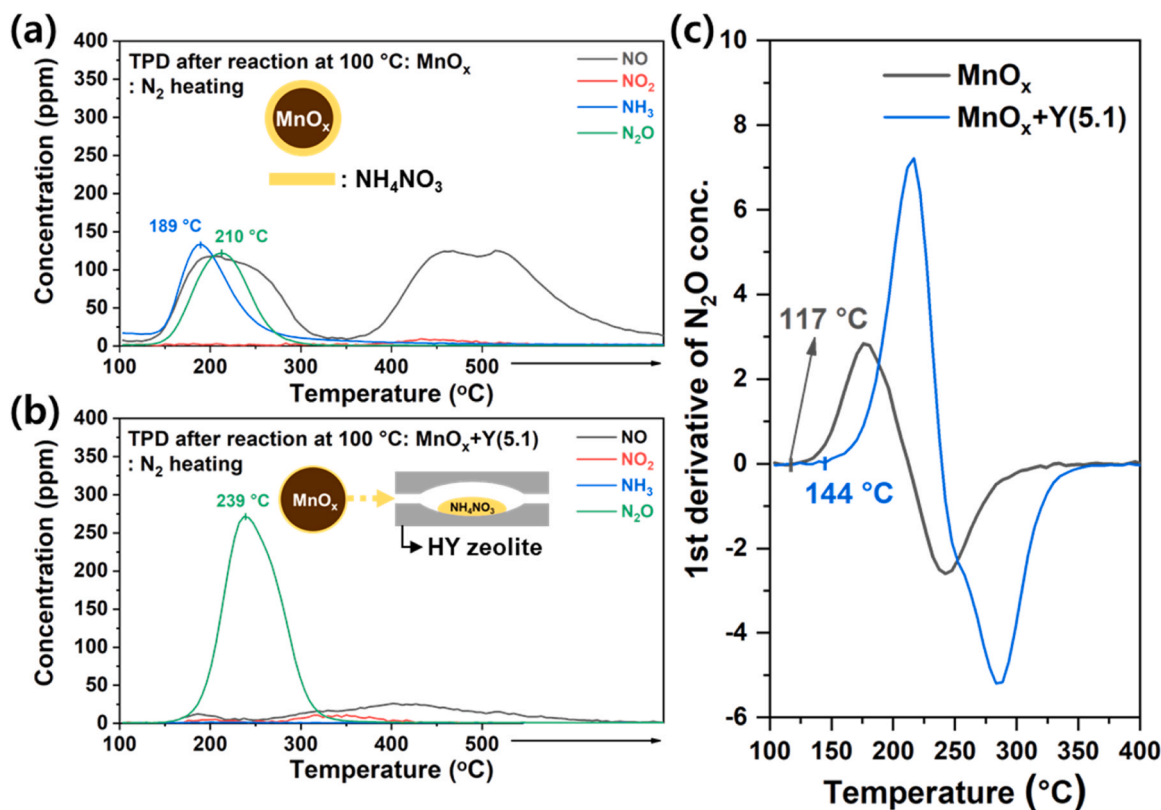
Fig. 8. The concentration profiles of temperature-programmed decomposition under N_2 atmosphere after NH_3-SCR reaction for 90 min at 100 °C over (a) MnO_x and (b) MnO_x+Y(5.1). The corresponding 1st derivative of N_2O concentration profiles is in (c).

produced via reaction (7), and a simultaneous NO oxidation reaction was entailed. Then, the N_2O peak centered at 136 °C, which was substantially lower than that detected under the N_2 atmosphere, was monitored. It signifies that the nitrate species under 500 ppm NO + 5 % O_2 atmosphere are less stable than those under just N_2. The NO consumption peaks over AN(5)/MnO_x were observed at 142 and 237 °C without forming any NO_2 peaks, which means that reaction (5) that produces NO_2 did not proceed at these temperatures. The NO consumption is supposed to be caused by the NH_3-SCR reaction owing to the reaction (6) that makes adsorbed NH_3 species. Above 250 °C, the NO consumption and NO_2 production occurred simultaneously, which is attributed to the NO oxidation reaction. For the AN/Y(5.1) sample (Fig. 7b), a small amount of N_2O was produced compared to the AN(5)/MnO_x sample. Note that a large amount of NH_4NO_3 was decomposed into N_2O and N_2 under the N_2 atmosphere in the results above (Fig. 6b). In contrast, the NH_4NO_3 over HY zeolite was not just thermally decomposed when NO and O_2 were fed to reactant gas. As NO was consumed as temperature increased, a similar amount of NO_2 was detected, indicating that the NH_4NO_3 was reduced by NO, followed by the rapid decomposition of NH_4NO_2 that finally produces NO_2, N_2, and H_2O (reaction (5)). After all the impregnated NH_4NO_3 was consumed (> 300 °C), the NO was oxidized to NO_2, which was not severe compared to that over MnO_x. Based on the TPD under N_2 and 500 ppm NO + 5 % O_2, it is concluded that the produced nitrate species over MnO_x could also diffuse into HY zeolite, producing intermediate species that can be stabilized in small pore structures and readily consumed by NO above 100 °C. Because of such diffusion of nitrate species and subsequent reduction by NO, the MnO_x+Y(5.1) sample could exhibit resistance to NH_4NO_3 deactivation, resulting in excellent NO_x conversion and N_2 selectivity. As shown in Fig. 5b, the catalytic activity of MnO_x+Y(5.1) was maintained without any deactivation for 22 h, while that of MnO_x steadily decreased due to the physical deposition of NH_4NO_3 on active sites. The TPD experiments were performed under an N_2 atmosphere

after the NH_3-SCR reaction. In order to deposit a sufficient amount of NH_4NO_3 on the catalysts and prevent thermal decomposition, a steady-state NH_3-SCR reaction was conducted for 90 min at 100 °C, followed by purging under an N_2 atmosphere to remove weakly adsorbed species. Then, the TPD experiments were conducted from 100 °C to 500 °C with a ramping rate of 10 °C min^{-1} under N_2 flow. The NO exhibited two broad peaks, and the NO_2 was barely detected for the MnO_x catalyst (Fig. 8a). The peaks assigned to NH_3 and N_2O appeared at 189 and 210 °C, respectively. When TPD was carried out over the MnO_x+Y(5.1) sample (Fig. 8b), a large part of NH_4NO_3 produced was decomposed into N_2O (reaction (8)), indicating that the other thermal decomposition routes were restrained upon physical mixing. Similar results were observed only when NH_4NO_3 was impregnated over zeolite Y sites rather than the MnO_x sample. If NH_4NO_3 were located in MnO_x after NH_3-SCR reaction and decomposed on MnO_x active sites even though the zeolite Y was physically mixed, it would not be possible to exhibit a concentration profile similar to that of the AN(5)/Y sample (Fig. 6b). Thus, the series of TPD experiments provides strong evidence that nitrate species produced during the NH_3-SCR reaction on the active site of MnO_x diffuse toward the HY zeolite domain. Moreover, similar to the TPD results of the AN-deposited catalyst, the N_2O peak position over the MnO_x+Y(5.1) sample (239 °C) was higher than that over MnO_x (210 °C). Based on the first derivative of the N_2O concentration profile (Fig. 8c), NH_4NO_3 formed over MnO_x started to degrade from 117 °C via reaction (8), whereas NH_4NO_3 decomposition commenced from 144 °C for MnO_x+Y(5.1) sample.

In addition to TPD analyses, the DRIFTS spectra obtained via 500 ppm NO + 5 % O_2 adsorption provide compelling evidence for the diffusion of nitrate and nitrite species from MnO_x to HY zeolite (Figure S7). When 500 ppm NO + 5 % O_2 was fed to MnO_x, one broad peak centered at 1370 cm^{-1} with shoulder at 1321 cm^{-1} was observed (Figure S7a). The peak of 1370 cm^{-1} is attributable to monodentate or bidentate nitrate species [31,32], and the 1321 cm^{-1} peak is assignable
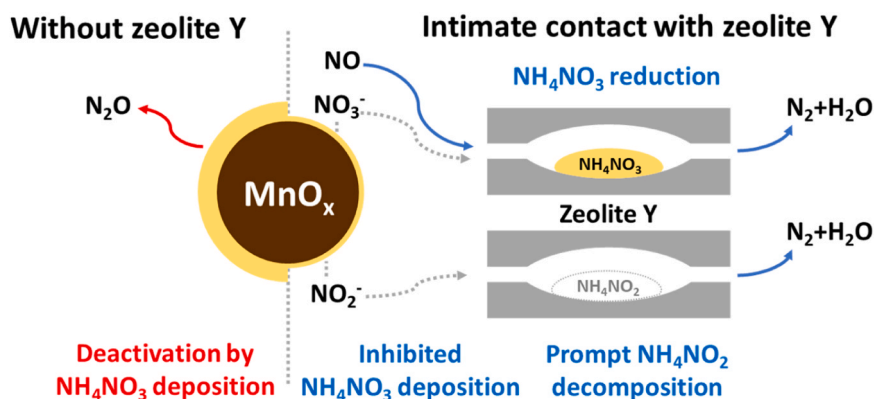
Scheme 1. The role of physically mixed H-form zeolite Y in metal oxide-zeolite hybrid catalysts for low-temperature NH_3-SCR reaction.

to monodentate nitrite species [33], confirming the formation of both nitrate and nitrite species over MnO_x active sites. In contrast to MnO_x, HY zeolite that has no oxidation ability exhibited no distinct peaks assigned to nitrate and nitrite species (Figure S7b). The $MnO_x+Y(5.1)$ sample showed completely different peaks compared to the MnO_x sample and HY zeolite (Figure S7c). Since NO would scarcely be activated over HY zeolite, those peaks do not arise from the HY zeolite of the $MnO_x+Y(5.1)$ mixture. In addition, if activated NO species is adsorbed to MnO_x among $MnO_x+Y(5.1)$, a similar trend to that of Figure S7a should be observed. Therefore, these observations subsidiarily suggest that the nitrate and nitrite species produced over MnO_x could be diffused toward HY zeolite.

Scheme 1 briefly describes our interpretation on the role of physically mixed H-form zeolite Y in the NH_3-SCR reaction. During NH_3-SCR reaction at low temperatures, NH_4NO_3 deposition is an important factor that should be considered since deposited NH_4NO_3 physically blocks the active sites of MnO_x catalysts, leading to decreased catalytic performance as reaction time elapsed. Moreover, these NH_4NO_3 species could be thermally decomposed over MnO_x, forming N_2O that deteriorates the N_2 selectivity. When MnO_x was physically mixed with HY zeolite with abundant Brønsted acid sites, it was found that the catalytic activity, N_2 selectivity, and stability at low-temperature operation were significantly enhanced via synergistic effect by physical mixing. The enhanced NO_x conversion is attributed to the diffusion of nitrite species toward the zeolite domain. As mentioned above, the abundant Brønsted acid sites in zeolite could catalyze the rapid decomposition of NH_4NO_2 into N_2 and H_2O. Moreover, the TPD results demonstrated that the nitrate species, which are deactivating materials by forming NH_4NO_3 on MnO_x, could also diffuse into the zeolite domain and form an NH_4NO_3 intermediate species stabilized by a microporous structure. Those intermediate species were not thermally decomposed into N_2O and H_2O but reacted with NO to produce N_2, H_2O, and NO_2, enhancing the catalytic activity, N_2 selectivity, and stability at low temperatures. We found that the critical factors affecting the diffusion of nitrite and nitrate species were the acidity of the zeolite and the extent of contact between MnO_x and zeolite. Our findings on understanding the diffusion and decomposition behavior of nitrite and nitrate species, respectively, will provide key information in manufacturing metal oxide-zeolite hybrid systems for the development of catalytic after-treatment technologies.

4. Conclusions

The hybrid catalyst consisting of physically mixed MnO_x and zeolite Y was prepared and applied to the low-temperature NH_3-SCR reaction. While the MnO_x catalyst showed low catalytic performance with continuous deterioration in activity as reaction time elapsed, superior catalytic activity with no deactivation was observed for the MnO_x+Y (5.1) sample. The significantly increased catalytic performance of the

$MnO_x+Y(5.1)$ sample is attributed to the diffusion of nitrite species to zeolite, followed by prompt decomposition of NH_4NO_2. That is, the decomposition rate of diffused nitrite species on Brønsted acid sites was much faster than acid sites on MnO_x. The induction period observed in the $MnO_x+Y(5.1)$ and the NH_3-SCR reaction results conducted under various conditions confirmed that the existence of H_2O in zeolite severely influences the diffusion and decomposition of nitrite species. In addition, it was verified that the decomposition of nitrite species demands more than a certain amount of acid sites. Based on the temperature-programmed decomposition of NH_4NO_3, we demonstrated that the nitrate species produced via the MnO_x active site can also be diffused into zeolite. The nitrate species could be stabilized via forming NH_4NO_3 in the micropore structure of HY zeolite, and those stabilized NH_4NO_3 were not thermally decomposed into N_2O and N_2 but reduced by NO, generating NH_4NO_2 that easily decomposed into N_2 and H_2O. In summary, the revealed role of bare H-form bare zeolite in the metal oxide-zeolite hybrid system was (1) the rapid decomposition of nitrite species compared to the acid sites of MnO_x and (2) the stabilization and facile reduction of diffused nitrate species by reacting with gaseous NO, which prevents the gradual deactivation of catalyst at low-temperature NH_3-SCR operation.

CRediT authorship contribution statement

Do Heui Kim: Writing – review & editing, Supervision, Funding acquisition. **Inhak Song:** Writing – review & editing. **Hongbeom Park:** Writing – review & editing, Investigation. **Hwangho Lee:** Writing – review & editing. **Hyun Sub Kim:** Writing – original draft, Visualization, Validation, Investigation, Conceptualization.

Declaration of Competing Interest

The authors declare that they have no known competing financial interests or personal relationships that could have appeared to influence the work reported in this paper.

Data availability

Data will be made available on request.

Acknowledgments

Appendix A. Supporting information

Supplementary data associated with this article can be found in the online version at doi:10.1016/j.apcatb.2024.124199.

References

[1] L. Han, S. Cai, M. Gao, J.-y Hasegawa, P. Wang, J. Zhang, L. Shi, D. Zhang, Selective catalytic reduction of NO_x with NH_3 by using novel catalysts: state of the art and future prospects, Chem. Rev. 119 (2019) 10916–10976, https://doi.org/10.1021/acs.chemrev.9b00202.

[2] F. Gao, X. Tang, H. Yi, S. Zhao, C. Li, J. Li, Y. Shi, X. Meng, A review on selective catalytic reduction of NO_x by NH_3 over Mn–based catalysts at low temperatures: catalysts, mechanisms, kinetics and DFT calculations, Catalysts 7 (2017) 199, https://doi.org/10.3390/catal7070199.

[3] H.S. Kim, H. Lee, H. Kim, S.W. Jeon, K.H. Hwang, D.H. Kim, Enhanced NH_3-SCR activity at low temperatures over MnO_x supported on two-dimensional TiO_2 derived from ZIF-8, J. Environ. Chem. Eng. 11 (2023) 110107, https://doi.org/10.1016/j.jece.2023.110107.

[4] D. Meng, W. Zhan, Y. Guo, Y. Guo, L. Wang, G. Lu, A highly effective catalyst of Sm-MnO_x for the NH_3-SCR of NO_x at low temperature: promotional role of Sm and its catalytic performance, ACS Catal. 5 (2015) 5973–5983, https://doi.org/10.1021/acscatal.5b00747.

[5] P. Sun, R.-t Guo, S.-m Liu, S.-x Wang, W.-g Pan, M.-y Li, The enhanced performance of MnO_x catalyst for NH_3-SCR reaction by the modification with Eu, Appl. Catal. A-Gen. 531 (2017) 129–138, https://doi.org/10.1016/j.apcata.2016.10.027.

[6] F. Gao, X. Tang, H. Yi, S. Zhao, J. Wang, Y. Shi, X. Meng, Novel Co– or Ni–Mn binary oxide catalysts with hydroxyl groups for NH_3–SCR of NO_x at low temperature, Appl. Surf. Sci. 443 (2018) 103–113, https://doi.org/10.1016/j.apsusc.2018.02.151.

[7] G. Qi, R.T. Yang, Performance and kinetics study for low-temperature SCR of NO with NH3 over MnO_x–CeO_2 catalyst, J. Catal. 217 (2003) 434–441, https://doi.org/10.1016/S0021-9517(03)00081-2.

[8] T. Andana, K.G. Rappé, F. Gao, J. Szanyi, X. Pereira-Hernandez, Y. Wang, Recent advances in hybrid metal oxide–zeolite catalysts for low-temperature selective catalytic reduction of NO_x by ammonia, Appl. Catal. B-Environ. 291 (2021) 120054, https://doi.org/10.1016/j.apcatb.2021.120054.

[9] I. Song, H. Lee, S.W. Jeon, I.A.M. Ibrahim, J. Kim, Y. Byun, D.J. Koh, J.W. Han, D.H. Kim, Simple physical mixing of zeolite prevents sulfur deactivation of vanadia catalysts for NO_x removal, Nat. Commun. 12 (2021) 901, https://doi.org/10.1038/s41467-021-21228-x.

[10] H. Lee, I. Song, S.W. Jeon, K.H. Hwang, D.H. Kim, Regeneration of a sulfur-poisoned selective catalytic reduction catalyst at ambient conditions, Appl. Catal. B-Environ. 341 (2024) 123333, https://doi.org/10.1016/j.apcatb.2023.123333.

[11] C. Yokoyama, M. Misono, Catalytic reduction of NO by propene in the presence of oxygen over mechanically mixed metal oxides and Ce-ZSM-5, Catal. Lett. 29 (1994) 1–6, https://doi.org/10.1007/BF00814245.

[12] M. Li, Y. Yeom, E. Weitz, W.M.H. Sachtler, An acid catalyzed step in the catalytic reduction of NO_x to N_2, Catal. Lett. 112 (2006) 129–132, https://doi.org/10.1007/s10562-006-0191-y.

[13] A.Y. Stakheev, G.N. Baeva, G.O. Bragina, N.S. Teleguina, A.L. Kustov, M. Grill, J.R. Thøgersen, Integrated DeNO$_x$–DeSoot catalytic systems with improved low-temperature performance, Top. Catal. 56 (2013) 427–433, https://doi.org/10.1007/s11244-013-9991-7.

[14] A.Y. Stakheev, A.I. Mytareva, D.A. Bokarev, G.N. Baeva, D.S. Krivoruchenko, A.L. Kustov, M. Grill, J.R. Thøgersen, Combined catalytic systems for enhanced low-temperature NO_x abatement, Catal. Today 258 (2015) 183–189, https://doi.org/10.1016/j.cattod.2015.05.023.

[15] M. Salazar, S. Hoffmann, O.P. Tkachenko, R. Becker, W. Grünert, Hybrid catalysts for the selective catalytic reduction of NO by NH_3: the influence of component separation on the performance of hybrid systems, Appl. Catal. B-Environ. 182 (2016) 213–219, https://doi.org/10.1016/j.apcatb.2015.09.028.

[16] M. Salazar, S. Hoffmann, V. Singer, R. Becker, W. Grünert, Hybrid catalysts for the selective catalytic reduction (SCR) of NO by NH_3. On the role of fast SCR in the reaction network, Appl. Catal. B-Environ. 199 (2016) 433–438, https://doi.org/10.1016/j.apcatb.2016.06.043.

[17] T. Andana, K.G. Rappé, N.C. Nelson, F. Gao, Y. Wang, Selective catalytic reduction of NO_x with NH_3 over Ce-Mn oxide and Cu-SSZ-13 composite catalysts – low temperature enhancement, Appl. Catal. B-Environ. 316 (2022) 121522, https://doi.org/10.1016/j.apcatb.2022.121522.

[18] N.C. Nelson, T. Andana, K.G. Rappé, Y. Wang, Mechanistic insight into low temperature SCR by ceria–manganese mixed oxides incorporated into zeolites, Catal. Sci. Technol. 13 (2023) 1111–1118, https://doi.org/10.1039/D2CY01921C.

[19] A. Grossale, I. Nova, E. Tronconi, D. Chatterjee, M. Weibel, The chemistry of the NO/NO_2–NH3 "fast" SCR reaction over Fe-ZSM5 investigated by transient reaction analysis, J. Catal. 256 (2008) 312–322, https://doi.org/10.1016/j.jcat.2008.03.027.

[20] I. Nova, C. Ciardelli, E. Tronconi, D. Chatterjee, B. Bandl-Konrad, NH_3–NO/NO_2 chemistry over V-based catalysts and its role in the mechanism of the Fast SCR reaction, Catal. Today 114 (2006) 3–12, https://doi.org/10.1016/j.cattod.2006.02.012.

[21] W. Zhu, X. Tang, F. Gao, H. Yi, R. Zhang, J. Wang, C. Yang, S. Ni, The effect of non-selective oxidation on the $Mn_2Co_1O_x$ catalysts for NH_3-SCR: positive and non-positive, Chem. Eng. J. 385 (2020) 123797, https://doi.org/10.1016/j.cej.2019.123797.

[22] S. Hong, S. Jin, Y. Deng, R. Garcia-Mendez, K.-i Kim, N. Utomo, L.A. Archer, Efficient scalable hydrothermal synthesis of MnO_2 with controlled polymorphs and morphologies for enhanced battery cathodes, ACS Energy Lett. 8 (2023) 1744–1751, https://doi.org/10.1021/acsenergylett.3c00018.

[23] I. Song, S. Youn, D.H. Kim, Characteristics of manganese supported on hydrous titanium oxide catalysts for the selective catalytic reduction of NO_x with ammonia, Top. Catal. 59 (2016) 1008–1012, https://doi.org/10.1007/s11244-016-0582-2.

[24] W. Song, Q. Cheng, L. Han, J. Ji, Y. Cai, W. Tan, J. Sun, C. Tang, L. Dong, Exploration of the Mn-O coordination regulated reaction stability of manganese oxides in NH_3-SCR: effect of deposited ammonium nitrates, Appl. Catal. B-Environ. (2023) 123607, https://doi.org/10.1016/j.apcatb.2023.123607.

[25] H. Kubota, C. Liu, T. Toyao, Z. Maeno, M. Ogura, N. Nakazawa, S. Inagaki, Y. Kubota, K.-i Shimizu, Formation and reactions of NH_4NO_3 during transient and steady-state NH_3-SCR of NO_x over H-AFX zeolites: spectroscopic and theoretical studies, ACS Catal. 10 (2020) 2334–2344, https://doi.org/10.1021/acscatal.9b05151.

[26] K. Khivantsev, J.-H. Kwak, N.R. Jaegers, I.Z. Koleva, G.N. Vayssilov, M.A. Derewinski, Y. Wang, H.A. Aleksandrov, J. Szanyi, Identification of the mechanism of NO reduction with ammonia (SCR) on zeolite catalysts, Chem. Sci. 13 (2022) 10383–10394, https://doi.org/10.1039/D2SC00350C.

[27] R. Gui, Q. Yan, T. Xue, Y. Gao, Y. Li, T. Zhu, Q. Wang, The promoting/inhibiting effect of water vapor on the selective catalytic reduction of NO_x, J. Hazard. Mater. 439 (2022) 129665, https://doi.org/10.1016/j.jhazmat.2022.129665.

[28] K. Khivantsev, N.R. Jaegers, L. Kovarik, J.C. Hanson, F. Tao, Y. Tang, X. Zhang, I.Z. Koleva, H.A. Aleksandrov, G.N. Vayssilov, Y. Wang, F. Gao, J. Szanyi, Achieving atomic dispersion of highly loaded transition metals in small-pore zeolite SSZ-13: high-capacity and high-efficiency low-temperature CO and passive NO_x adsorbers, Angew. Chem. -Int. Ed. 57 (2018) 16672–16677, https://doi.org/10.1002/anie.201809343.

[29] I. Song, H. Lee, S.W. Jeon, D.H. Kim, Controlling catalytic selectivity mediated by stabilization of reactive intermediates in small-pore environments: a study of Mn/TiO_2 in the NH_3-SCR reaction, ACS Catal. 10 (2020) 12017–12030, https://doi.org/10.1021/acscatal.0c03154.

[30] S. Chaturvedi, P.N. Dave, Review on thermal decomposition of ammonium nitrate, J. Energ. Mater. 31 (2013) 1–26, https://doi.org/10.1080/07370652.2011.573523.

[31] F. Lin, Q. Wang, J. Zhang, J. Jin, S. Lu, J. Yan, Mechanism and kinetics study on low-temperature NH_3-SCR over manganese–cerium composite oxide catalysts, Ind. Eng. Chem. Res. 58 (2019) 22763–22770, https://doi.org/10.1021/acs.iecr.9b04780.

[32] X. Xiao, J. Wang, X. Jia, C. Ma, W. Qiao, L. Ling, Low-temperature selective catalytic reduction of NO_x with NH_3 over Mn–Ce composites synthesized by polymer-assisted deposition, ACS Omega 6 (2021) 12801–12812, https://doi.org/10.1021/acsomega.1c01123.

[33] X. Hu, Q. Shi, H. Zhang, P. Wang, S. Zhan, Y. Li, NH_3-SCR performance improvement over Mo modified Mo(x)-MnO_x nanorods at low temperatures, Catal. Today 297 (2017) 17–26, https://doi.org/10.1016/j.cattod.2017.06.015.